

# Application of supersymmetric quantum mechanics to study bound state properties of exotic hypernuclei

*Md. Abdul Khan*

*Department of Physics, Aliah University,  
AA-II, Plot No. IIA/27, Newtown, Kolkata-700156, West Bengal, India.  
Email: drakhan.rsm.phys@gmail.com; drakhan.phys@aliah.ac.in*

## Abstract

Bound state properties of few single and double- $\Lambda$  hypernuclei is critically examined in the framework of core- $\Lambda$  and core+ $\Lambda + \Lambda$  few-body model applying hyperspherical harmonics expansion method (HHEM). The  $\Lambda\Lambda$  potential is chosen phenomenologically while the core- $\Lambda$  potential is obtained by folding a phenomenological  $\Lambda N$  interaction into the density distribution of the core. The depth of the effective  $\Lambda N$  potential is adjusted to reproduce the experimental data for the core- $\Lambda$  subsystem. The three-body Schrödinger equation is solved by hyperspherical adiabatic approximation (HAA) to get the ground state energy and wave function. The ground state wavefunction is used to construct the supersymmetric partner potential following prescription of supersymmetric quantum mechanics (SSQM) algebra. The newly constructed supersymmetric partner potential is used to solve the three-body Schrödinger equation to get the energy and wavefunction for the first excited state of the original potential. The method is repeated to predict energy and wavefunction of the next higher excited states. The possible number of bound states is found to increase with the increase in mass of the core of the hypernuclei. The Root Mean Squared (RMS) matter radius and some other relevant geometrical observables are also predicted.

PACS 21.80.+a; 21.60.Jz; 21.30.Fe

**Key words:**

Hypernuclei, Few Body System (FBS), Hyperspherical Harmonics (HH), Hyperspherical Harmonics Expansion (HHE), Super Symmetric Quantum Mechanics (SSQM).

# I Introduction

Since the discovery of the light exotic hypernuclei in the early sixties [1-2], peoples are giving much attention to study the structure of such multistrange hypernuclei [3-4]. Some of the experimentally observed one- and two- $\Lambda$  hypernuclei are  ${}^5_{\Lambda}\text{He}$ ,  ${}^6_{\Lambda\Lambda}\text{He}$ ,  ${}^9_{\Lambda}\text{Be}$ ,  ${}^{10}_{\Lambda\Lambda}\text{Be}$ ,  ${}^{13}_{\Lambda}\text{C}$  and  ${}^{13}_{\Lambda\Lambda}\text{B}$  [5-11]. Information about the  $\Lambda\Lambda$  and  $\Lambda N$  forces can be extracted from the bound state properties of such nuclei. These informations on  $\Lambda\Lambda$  and  $\Lambda N$  interaction together with the well known  $NN$  interaction may give better understanding of the strong quark-quark (qq) interaction, since the hyperons also have qq structure as that of nucleons. As for example proton has three quarks namely up,up,down ( $p \rightarrow uud$ ), neutron has quarks up,down,down ( $n \rightarrow udd$ ),  $\Lambda^0$  has quarks up,down,strange ( $\Lambda^0 \rightarrow uds$ ) etc. In the earlier stage of their discovery, emulsion experiments provided some information on the binding energies of  $\Lambda$ -particle in the light exotic hypernuclei and their decay rates (life times  $\sim 10^{-10}\text{sec}$ ) [2]. From the available binding energy data physicists gathered some qualitative informations about the  $\Lambda$ -nucleon ( $\Lambda N$ ) interaction and single particle potential strength for the  $\Lambda$ -particle in hypernuclei [12]. The hyperon-nucleon scattering experiments have also been performed but these are not so profound and are still in the primary stages and do not give detailed phase shifts to construct the potential reliably. Some  $\Lambda N$  and  $\Sigma N$  total cross-sections and very few angular distribution at low energies have been measured [13-18], but these are not sufficient to allow the phase shift analysis. Under the circumstances, the bound state properties of single- and double-  $\Lambda$  hypernuclei can only give useful indirect information about  $\Lambda N$  and  $\Lambda\Lambda$  interactions. For example, one can take phenomenological forms of  $\Lambda N$  and  $\Lambda\Lambda$  interactions and see if they reproduce the experimentally observed observables of the hypernuclei. Alternatively one can adjust the parameters of the empirical potential to reproduce the bound state properties and thus predict the effective  $\Lambda N$  and  $\Lambda\Lambda$  interactions. In some earlier works [19-22] physicists have used variational and approximate few body methods for the hypernuclei treating them a few body system. In the present work, we investigate the structure and properties of the ground and excited states of double- $\Lambda$  hypernuclei with mass number  $A = 6, 8, 34, 42, 92$  and ground state of their binary subsystems consisting the core and one outer core  $\Lambda$  hyperon. A simple two-body model has been adopted here for the single- $\Lambda$  hypernucleus ( $A = A_c + 1$ ) consisting of a  $A_c = 4, 6, 30, 40, 90$  core and one valence  $\Lambda$  particle. And for the double- $\Lambda$  hypernuclei ( $A = A_c + 2$ ), we adopt a three-body model consisting core of mass  $A_c (=4,6,30,40,90)$  and two valence  $\Lambda$  particles. For  $\Lambda\Lambda$  potential a phenomenological form has been chosen. The core- $\Lambda$  potential has been obtained by folding an effective  $\Lambda N$  potential by the density of the core nucleus. The strength of the effective  $\Lambda N$  potential for a given core is adjusted to reproduce the experimentally known BE of the single  $\Lambda$  hypernuclei  ${}^5_{\Lambda}\text{He}$ ,  ${}^7_{\Lambda}\text{He}$  [6],  ${}^7_{\Lambda}\text{Be}$  [23],  ${}^{33}_{\Lambda}\text{S}$  [24],  ${}^{41}_{\Lambda}\text{Ca}$  [24] and  ${}^{91}_{\Lambda}\text{Zr}$  [25]. The same folded core- $\Lambda$  potential is then used for the double- $\Lambda$  hypernucleus for the same core.

We used hyperspherical harmonics expansion (HHE) method to solve the three-body system. This method is a powerful tool for the *ab initio* solution of the few body Schrödinger equation for a given set of binary interaction potentials among the constituent particles. This method has been used for bound states in atomic [26-33], nuclear [34-40] and particle physics [41-43]. Attempts have been made to use it in scattering problems as well [44]. In this method, the wave function is expanded in a complete set of hyperspherical harmonics (HH), which are, for a three-body system, the six-dimensional analogue of ordinary spherical harmonics. The Schrödinger equation reduces to a set of coupled differential equations which can be solved numerically. The HHE method is essentially exact and involves no approximation other than an eventual truncation of the expansion basis. Any desired precision in the binding energy can, in principle, be achieved by gradually expanding the expansion basis and checking the rate of convergence. However the number of coupled differential equations and hence, the complexity in the numerical solution increases rapidly as the expansion basis is increased by introducing larger hyper angular momentum quantum numbers. Computer limitations set an ultimate limit to the precision attainable.

We have calculated the two- $\Lambda$  separation energy ( $B_{\Lambda\Lambda}$ ),  $\Lambda\Lambda$  bond energy ( $\Delta B_{\Lambda\Lambda}$ ) and some size parameters for all the above double  $\Lambda$  hypernuclei. Here  $B_{\Lambda\Lambda}$  and  $\Lambda\Lambda$  bond energy  $\Delta B_{\Lambda\Lambda}$  are defined as

$$B_{\Lambda\Lambda}(^A_{\Lambda\Lambda}Z) = [M(^{A-2}Z) + 2M_\Lambda - M(^A_{\Lambda\Lambda}Z)]c^2 \quad (1)$$

and

$$\Delta B_{\Lambda\Lambda} = B_{\Lambda\Lambda}(^A_{\Lambda\Lambda}Z) - 2B_\Lambda(^{A-1}Z) \quad (2)$$

As the ground state BE is quite large, one may expect the excited states to be observable experimentally, although they have not been reported so far. However, the HHE method is known for its rather slow convergence, which is especially manifested in the excited states. The excited state wave function is more spread out than the ground state and therefore needs larger  $K_{max}$  for the same degree of convergence. We circumvent this difficulty by invoking supersymmetric quantum mechanics (SSQM) [45]. In SSQM, we construct the supersymmetric partner potential ( $V_2$ ) of the original potential ( $V_1$ ) [1]. According to SSQM, the spectra of  $V_1$  and  $V_2$  are identical except for the absence of the ground state of  $V_1$  in the spectrum of  $V_2$  [45]. Hence the ground state of  $V_2$  corresponds to the first excited state of  $V_1$ . Thus we can solve for the ground state of  $V_2$ , whose convergence is fast (being a ground state). Its BE is the BE of the first excited state of the original potential. The wave function of the first excited state of  $V_1$  can be obtained by applying an appropriate operator on the ground state wave function of  $V_2$ .

The paper is organized as follows: In section II, we review the HHE method for a three-body system consisting of non identical particles with a brief review of SSQM. Results of calculation and discussion are presented in section III. Finally in section IV we draw our conclusions.

## II Use of hyperspher spherical harmonics expansion method and super symmetric quantum mechanics

We treat each of the six double- $\Lambda$  hypernuclei  $^6_{\Lambda\Lambda}\text{He}$ ,  $^8_{\Lambda\Lambda}\text{Be}$ ,  $^8_{\Lambda\Lambda}\text{He}$ ,  $^{34}_{\Lambda\Lambda}\text{S}$ ,  $^{42}_{\Lambda\Lambda}\text{Ca}$ ,  $^{92}_{\Lambda\Lambda}\text{Zr}$  as a three body system, where each of the core  $^4\text{He}$ ,  $^6\text{Be}$ ,  $^6\text{He}$ ,  $^{32}\text{S}$ ,  $^{40}\text{Ca}$ ,  $^{90}\text{Zr}$  is labeled as particle 1 and the two valence  $\Lambda$  hyperons as particles 2 and 3 respectively (see Fig. 1).

For a given partition  $i$  (in which  $i$  is the spectator), a set of Jacobi co-ordinates is defined as:

$$\left. \begin{aligned} \vec{x}_i &= \left[ \frac{m_j m_k M}{m_i (m_j + m_k)^2} \right]^{\frac{1}{4}} (\vec{r}_j - \vec{r}_k) \\ \vec{y}_i &= \left[ \frac{m_i (m_j + m_k)^2}{m_j m_k M} \right]^{\frac{1}{4}} \left( \vec{r}_i - \frac{m_j \vec{r}_j + m_k \vec{r}_k}{m_j + m_k} \right) \\ \vec{R} &= \frac{1}{M} (m_i \vec{r}_i + m_j \vec{r}_j + m_k \vec{r}_k) \end{aligned} \right\} \quad (3)$$

for (i,j,k)=(1,2,3 cyclic). Here  $m_i$ ,  $\vec{r}_i$  are the mass and position of the  $i^{\text{th}}$  particle and  $M = m_i + m_j + m_k$ .  $\vec{R}$  is the coordinate of the centre of mass of the system. Since the interactions among the constituent particles depend only on their relative separations, the centre of mass motion separates out automatically. Thus the relative motion of the three-body system is described by the Schrödinger equation

$$\left[ -\frac{\hbar^2}{2\mu} (\nabla_{x_i}^2 + \nabla_{y_i}^2) + V_{jk}(\vec{x}_i) + V_{ki}(\vec{x}_i, \vec{y}_i) + V_{ij}(\vec{x}_i, \vec{y}_i) - E \right] \Psi(\vec{x}_i, \vec{y}_i) = 0 \quad (4)$$

where  $\mu = \left[ \frac{m_i m_j m_k}{M} \right]^{\frac{1}{2}}$  is an effective mass parameter and  $V_{ij}$  is the interaction potential between particles  $i$  and  $j$ . In terms of the hyperspherical variables [40]

$$\left. \begin{aligned} x_i &= \rho \cos \Phi_i \\ y_i &= \rho \sin \Phi_i \end{aligned} \right\} \quad (5)$$

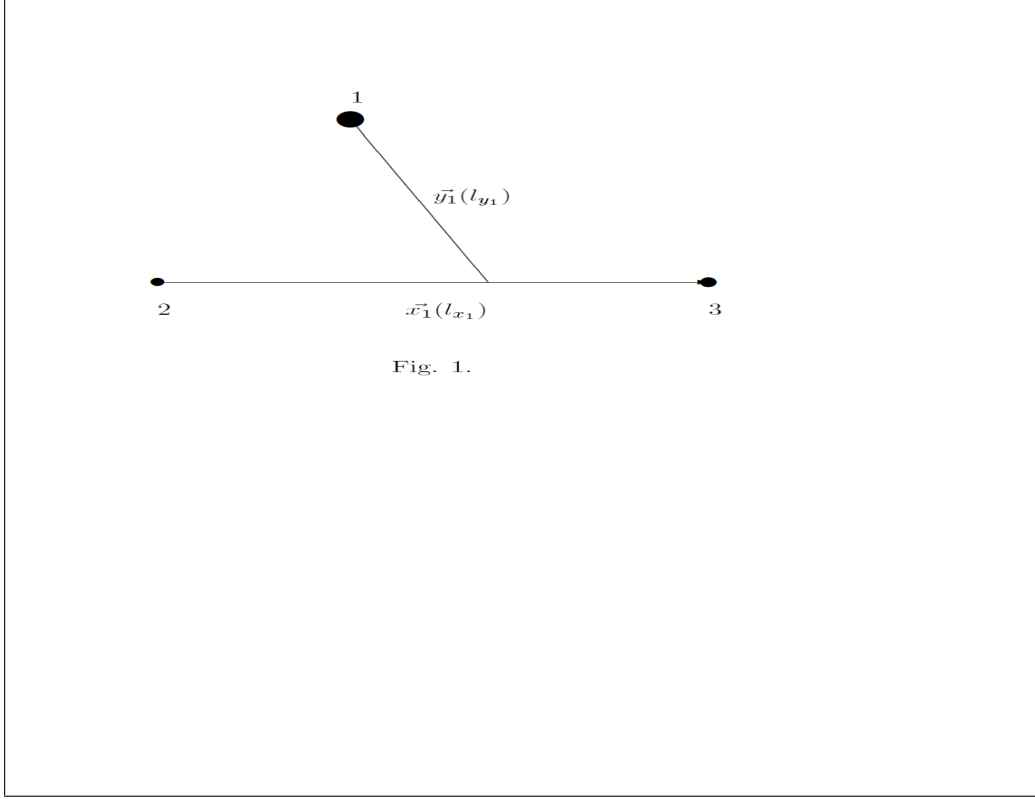


Fig. 1.

Figure 1: Choice of Jacobi coordinates for the partition 1.

the Schrödinger equation becomes

$$\left[ -\frac{\hbar^2}{2\mu} \left\{ \frac{1}{\rho^5} \frac{\partial}{\partial \rho} (\rho^5 \frac{\partial}{\partial \rho}) - \frac{\hat{\mathcal{K}}^2(\Omega_i)}{\rho^2} \right\} + V(\rho, \Omega_i) - E \right] \Psi(\rho, \Omega_i) = 0, \quad (6)$$

where the hyper-radius  $\rho$  is invariant under three-dimensional rotations and permutations of the particle indices. The five hyper angles constituted by polar angles  $(\theta_{x_i}, \phi_{x_i})$  of  $\vec{x}_i$ , polar angles  $(\theta_{y_i}, \phi_{y_i})$  of  $\vec{y}_i$  and the angle  $\Phi_i$ , are collectively denoted by  $\Omega_i \rightarrow \{\Phi_i, \theta_{x_i}, \theta_{y_i}, \phi_{x_i}, \phi_{y_i}\}$ . Thus  $(\rho, \Omega_i)$  constitutes the six hyperspherical variables of which the five hyper angles  $\Omega_i$  depend on the choice of partition  $i$ . In the above equation  $V(\rho, \Omega_i) = V_{jk}(\vec{x}_i) + V_{ki}(\vec{x}_i, \vec{y}_i) + V_{ij}(\vec{x}_i, \vec{y}_i)$  is the total interaction potential expressed in terms of the hyperspherical variables in the partition  $i$  and  $\hat{\mathcal{K}}^2(\Omega_i)$  is the square of hyper angular momentum operator given by [40]

$$\hat{\mathcal{K}}^2(\Omega_i) = -\frac{\partial^2}{\partial \Phi_i^2} - 4 \cot 2\Phi_i \frac{\partial}{\partial \Phi_i} + \frac{1}{\cos^2 \Phi_i} \hat{l}^2(\hat{x}_i) + \frac{1}{\sin^2 \Phi_i} \hat{l}^2(\hat{y}_i), \quad (7)$$

where  $\hat{l}^2(\hat{x}_i)$  and  $\hat{l}^2(\hat{y}_i)$  are the squares of ordinary orbital angular momentum operators associated with  $\vec{x}_i$  and  $\vec{y}_i$  motions respectively. The operator  $\hat{\mathcal{K}}^2$  satisfies an eigenvalue equation [40]

$$\hat{\mathcal{K}}^2(\Omega_i) \mathcal{Y}_{K\alpha_i}(\Omega_i) = K(K+4) \mathcal{Y}_{K\alpha_i}(\Omega_i). \quad (8)$$

Here  $K (= 2n_i + l_{x_i} + l_{y_i}, n_i$  being a non-negative integer) represents the hyper angular momentum quantum number and  $\alpha_i \equiv \{l_{x_i}, l_{y_i}, L, M\}$  is a short hand notation, in which  $L$  and  $M$  denote the total orbital angular momentum and its projection, respectively. The normalized eigen functions  $\mathcal{Y}_{K\alpha_i}(\Omega_i)$  are called the hyperspherical harmonics (HH) and these depend on the choice of partition. A detailed analytic expression for  $\mathcal{Y}_{K\alpha_i}(\Omega_i)$

can be found in [40]. In the HHE method,  $\Psi(\rho, \Omega_i)$  is expanded in the complete set of HH corresponding to the partition  $i$ :

$$\Psi(\rho, \Omega_i) = \sum_{K\alpha_i} \frac{U_{K\alpha_i}(\rho)}{\rho^{5/2}} \mathcal{Y}_{K\alpha_i}(\Omega_i). \quad (9)$$

Substitution of Eq. (9) in Eq. (6) and the use of orthonormality of HH leads to a set of coupled differential equations (CDE) in  $\rho$

$$\left[ -\frac{\hbar^2}{2\mu} \left( \frac{d^2}{d\rho^2} - \frac{\mathcal{L}_K(\mathcal{L}_K+1)}{\rho^2} \right) - E \right] U_{K\alpha_i}(\rho) + \sum_{K'\alpha_i' < K\alpha_i} V(\rho, \Omega_i) |K'\alpha_i' \rangle U_{K'\alpha_i'}(\rho) = 0, \quad (10)$$

where  $\mathcal{L}_K = K + 3/2$  and

$$\langle K\alpha_i | V(\rho, \Omega_i) | K'\alpha_i' \rangle = \int_{\Omega_i} \mathcal{Y}_{K\alpha_i}^*(\Omega_i) V(\rho, \Omega_i) \mathcal{Y}_{K'\alpha_i'}(\Omega_i) d\Omega_i. \quad (11)$$

The number of coupled differential equations to be solved, Eq. (10) is in principle, an infinite one, which arises out of an infinite number of basis states Eq. (9). For practical computation, the hyperspherical harmonics expansion basis in Eq. (9) is truncated to a finite set by retaining all values of  $K$  up to a maximum  $K_{max}$ . For a given  $K$ , all allowed values of the set of quantum numbers  $\alpha_i$  are included. The basis states is further reduced by imposing the constraints arising out of symmetry requirements and associated conserved quantum numbers. Thus the infinite set of CDE is now reduced to a finite set. This finite set of CDE is solved numerically by hyperspherical adiabatic approximation [31,46] which is based on the idea of adiabatic separation of hyper-angular motions from the hyper-radial one. In this procedure the potential matrix  $\langle K\alpha_i | V | K'\alpha_i' \rangle$  together with the diagonal hyper-centrifugal term is diagonalized for a fixed value of  $\rho$ . The lowest eigenvalue  $\omega_0(\rho)$  and the corresponding eigenvector  $\chi_{K\alpha_i,0}(\rho)$  are obtained as parametric function of  $\rho$ . Then the set of CDE, Eq. (10) is approximately decoupled into a single ordinary differential equation

$$\left[ -\frac{\hbar^2}{2\mu} \frac{d^2}{d\rho^2} + \omega_0(\rho) - E \right] \psi(\rho) = 0 \quad (12)$$

Numerical solution of Eq. (12), subject to appropriate boundary conditions gives the ground state energy  $E$  and partial waves of the three-body system. The partial waves are given by

$$U_{K\alpha_i}(\rho) \simeq \psi_0(\rho) \chi_{K\alpha_i,0}(\rho) \quad (13)$$

We now present a brief review of properties of supersymmetric quantum mechanics (SSQM) [45] used here to calculate the observables for the excited states. Let us consider a one dimensional Schrödinger equation of the form

$$\left[ -\frac{\hbar^2}{2\mu} \frac{d^2}{d\rho^2} + V(\rho) - E \right] \psi(\rho) = 0 \quad (14)$$

For the single- $\Lambda$  hypernuclei,  $V(\rho)$  is just the  $\Lambda$ -core potential plus the centrifugal term and  $\rho$  is the core- $\Lambda$  separation. For double- $\Lambda$  hypernuclei  $V(\rho)$  is the lowest eigen potential  $\omega_0(\rho)$  and  $\rho$  is the hyper-radius. Suppose the ground state energy is  $E_0$ . We shift the energy scale by  $E_0$ , such that the ground state is at zero energy and the corresponding potential is renamed  $V_1(\rho) (=V(\rho) - E_0)$ . Then for the ground state

$$\left[ -\frac{\hbar^2}{2\mu} \frac{d^2}{d\rho^2} + V_1(\rho) \right] \psi_0(\rho) = 0 \quad (15)$$

From this we get

$$V_1(\rho) = \frac{\hbar^2 \psi_0''(\rho)}{2\mu \psi_0(\rho)} \quad (16)$$

Let us now define a super potential,  $W(\rho)$  as

$$W(\rho) = -\frac{\hbar}{\sqrt{2\mu}} \frac{\psi_0'(\rho)}{\psi_0(\rho)} \quad (17)$$

and two operators

$$\left. \begin{aligned} A &= \frac{\hbar}{\sqrt{2\mu}} \frac{d}{d\rho} + W(\rho) \\ A^\dagger &= -\frac{\hbar}{\sqrt{2\mu}} \frac{d}{d\rho} + W(\rho) \end{aligned} \right\} \quad (18)$$

Then one can easily check that

$$V_1(\rho) = W^2(\rho) - \frac{\hbar}{\sqrt{2\mu}} W'(\rho) \quad (19)$$

and

$$H_1 \equiv -\frac{\hbar^2}{2\mu} \frac{d^2}{d\rho^2} + V_1(\rho) = A^\dagger A \quad (20)$$

Here  $H_1$  is the original Hamiltonian in the shifted energy scale. We next define a partner Hamiltonian

$$H_2 = AA^\dagger = \frac{\hbar^2}{2\mu} \frac{d^2}{d\rho^2} + V_2(\rho), \quad (21)$$

in which the partner potential is given by

$$V_2(\rho) = W^2(\rho) + \frac{\hbar}{\sqrt{2\mu}} W'(\rho). \quad (22)$$

Let us denote the  $n^{\text{th}}$  eigenvalue and corresponding eigen function of  $H_2$  by  $E_n^{(2)}$  and  $\psi_n^{(2)}(\rho)$  respectively, while the  $n^{\text{th}}$  eigenvalue and corresponding eigenfunction of  $H_1$  are denoted by  $E_n$  and  $\psi_n(\rho)$  respectively. Then it is easily verified that

$$H_2(A\psi_n) = AA^\dagger A\psi_n = AH_1\psi_n = E_n(A\psi_n), \quad (23)$$

which means that  $A\psi_n$  is an eigenfunction of  $H_2$  corresponding to energy  $E_n$ . Similarly

$$H_1(A^\dagger\psi_n^{(2)}) = A^\dagger AA^\dagger\psi_n^{(2)} = A^\dagger H_2\psi_n^{(2)} = E_n^{(2)}(A^\dagger\psi_n^{(2)}) \quad (24)$$

Thus  $A^\dagger\psi_n^{(2)}$  is an eigenfunction of  $H_1$  corresponding to energy  $E_n^{(2)}$ . Now from Eq. (17) and (18)

$$A\psi_0 = 0. \quad (25)$$

Thus  $A\psi_0$  is a trivial solution of Eq. (23). The ground state of  $H_2$  will thus be  $A\psi_1$  corresponding to energy  $E_1$  (note that  $E_0 < E_1 \leq E_2 \leq E_3 \leq \dots$ ). Hence  $E_0^{(2)} = E_1$ , and from Eq. (24),  $\psi_1 \propto A^\dagger\psi_0^{(2)}$ . Thus if we solve for the ground state of  $V_2(\rho)$ , we get the energy  $E_1$  (in shifted energy scale), which is the energy of the first excited state of  $V_1(\rho)$ . It is easily seen that the corresponding normalized eigenfunction is

$$\psi_1(\rho) = \frac{1}{\sqrt{E_1}} A^\dagger\psi_0^{(2)}. \quad (26)$$

Hence we numerically solve Eq. (14) for the ground state and calculate the superpotential  $W(\rho)$  and the partner potential  $V_2(\rho)$  according to Eq. (17) and (22) respectively. Then we solve the same Schrödinger equation with  $V_2(\rho)$  to obtain  $E_0^{(2)}$  and  $\psi_0^{(2)}$ . From  $\psi_0^{(2)}$ , we get  $\psi_1(\rho)$  using eq(26). Finally the energy of the first excited state of  $V_1(\rho)$  is obtained by back shifting  $E_0^{(2)}$ .

### III Results and Discussions

In the present calculation we have taken the core to be structureless. Since the core ( ${}^4\text{He}$ ,  ${}^6\text{Be}$ ,  ${}^6\text{He}$ ,  ${}^{32}\text{S}$ ,  ${}^{40}\text{Ca}$ ,  ${}^{90}\text{Zr}$ ) contains only nucleons and no  $\Lambda$ -particles, there is no symmetry requirements under exchange of the valence  $\Lambda$  particles with the core nucleons. The only symmetry requirements are (i) anti-symmetrization of the core wave function under exchange of the nucleons and (ii) anti-symmetrization of the three body wave function under exchange of the two  $\Lambda$  particles. The former is implicitly taken care of by the choice of the core as a building block. For double- $\Lambda$  hypernuclei, the latter is correctly incorporated by restricting the  $l_{x_1}$  values, explained in the following. Thus, within the three-body model, the symmetry requirements are correctly satisfied without any approximation. For the single- $\Lambda$  hypernuclei, there are no symmetry requirements. The ground state of all experimentally known double- $\Lambda$  hypernuclei have a total angular momentum quantum number  $J = 0$  and even (or positive) parity. We assume this to be true for all double- $\Lambda$  hypernuclei with core having  $N = \text{even}$ ,  $Z = \text{even}$ . The possible total spin (S) of the three-body system (*core* +  $\Lambda$  +  $\Lambda$ ) can take two values 0 or 1 since the spin of the core in all the above cases has a value 0. Thus the total orbital angular momentum L can be either 0 or 1 corresponding to S=0 or 1 respectively. Hence the set of quantum numbers (LS)J for the ground state of all even-even core double- $\Lambda$  hypernuclei is (00)0 and (11)0 which corresponds to  ${}^1S_0$  and  ${}^3P_0$  states. Since the ground state of these nuclei have definite parity, odd and even parity states will not mix. In our case, the ground state of all the six double- $\Lambda$  hypernuclei is a pure  ${}^1S_0$  state. Since the core is spin less, the spin singlet state (S=0) corresponds to zero total spin of the valence  $\Lambda$ - particles (i.e.  $S_{23}=0$ ). Hence the spin part of the wave function is antisymmetric under the exchange of the spins of the two  $\Lambda$ -particles. Thus the spatial part must be symmetric under the exchange of the two  $\Lambda$ -hyperons. The symmetry of the spatial part is determined by the hyper spherical harmonics, since the hyper radius  $\rho$  and hence the hyper radial partial waves ( $U_{K\alpha}(\rho)$ ) are invariant under permutation of the particles. Under the pair exchange operator  $P_{23}$  which interchanges particles 2 and 3,  $\vec{x}_1 \rightarrow -\vec{x}_1$  and  $\vec{y}_1$  remains unchanged (see Eq. (3)). Consequently  $P_{23}$  acts like the parity operator for (23) pair only. Choosing the two valence  $\Lambda$ -hyperons to be in spin singlet state (spin antisymmetric), the space wave function must be symmetric under  $P_{23}$ . This then requires  $l_{x_1}$  to be even. For the spin singlet state total orbital angular momentum, L=0, hence we must have  $l_{x_1} = l_{y_1} = \text{even integer}$ . Since  $K = 2n_1 + l_{x_1} + l_{y_1}$ , where  $n_1$  is a non-negative integer,  $K$  must be even and

$$l_{x_1} = l_{y_1} = \left. \begin{array}{l} 0, 2, 4, \dots, K/2 \quad \text{if } K/2 \text{ is even} \\ 0, 2, 4, \dots, (K/2 - 1) \quad \text{if } K/2 \text{ is odd} \end{array} \right\}. \quad (27)$$

Again for the triplet state (S=1), the two valence  $\Lambda$ -hyperons will be in spin triplet state ( $S_{23} = 1$ , spin symmetric). Hence the space wave function must be antisymmetric under  $P_{23}$ . This then requires  $l_{x_1}$  to be odd. For the spin triplet state, the total orbital angular momentum, L=1, hence  $l_{y_1}$  may take values  $l_{x_1}$  and  $l_{x_1} \pm 1$  (and only 1 if  $l_{x_1} = 0$ ) but the parity conservation allows  $l_{y_1}=l_{x_1}$  only (except  $l_{x_1} = 0$ ). Again since  $K = 2n_1 + l_{x_1} + l_{y_1}$ , where  $n_1$  is a non-negative integer,  $K$  must be even ( $K \neq 0$ ) and

$$l_{x_1} = l_{y_1} = \left. \begin{array}{l} 1, 3, 5, \dots, K/2 \quad \text{if } K/2 \text{ is odd} \\ 1, 3, 5, \dots, (K/2 - 1) \quad \text{if } K/2 \text{ is even} \end{array} \right\}. \quad (28)$$

For a practical calculation, the HH expansion basis (eq(9)) is truncated to a maximum value ( $K_{max}$ ) of K. For each allowed  $K \leq K_{max}$  with K=even integers, all allowed values of  $l_{x_1}$  are included. The even values of  $l_{x_1}$  correspond to L=0, S=0 and odd values of  $l_{x_1}$  correspond to L=1, S=1. This truncates eq(10) to a set of N coupled differential equations, where

$$N = \left. \begin{array}{l} \left( \frac{K_{max}}{2} + 1 \right) \left( \frac{K_{max}}{4} + 1 \right) \quad \text{if } K_{max}/2 \text{ is even} \\ \left( \frac{K_{max}+2}{4} \right) \left( \frac{K_{max}}{2} + 2 \right) \quad \text{if } K_{max}/2 \text{ is odd} \end{array} \right\}, \quad (29)$$

which will be solved by the hyperspherical adiabatic approximation (HAA) [46].

Since realistic  $\Lambda\Lambda$  potential is not available at this stage. We used phenomenological three term Gaussian  $\Lambda\Lambda$  potential with parameters adjusted to reproduce the experimental data for known double- $\Lambda$  hypernuclei. The  $\Lambda\Lambda$  potential used here is given by

$$V_{\Lambda\Lambda}(r) = \sum_{i=1}^3 V_i \exp\left(-\frac{r^2}{\beta_i^2}\right). \quad (30)$$

The parameters of this potential are presented in Table I. A short range repulsive term in the  $\Lambda\Lambda$  potential is included to simulate Pauli principle between the valence  $\Lambda$  particles. The core- $\Lambda$  potential is obtained by folding phenomenological  $\Lambda$ -nucleon potential into the density distribution of the core nucleus. The chosen density distribution function of the core is given by

$$\rho(r) = \frac{\rho_0}{1 + \exp\left(\frac{r-r_c}{a}\right)} \quad (31)$$

with  $r_c = r_0 A_c^{1/3}$  fm,  $a = 0.65$  fm,  $r_0 = 1.7$  fm (where  $r_c$  is termed the half density radius and  $a$ , the skin thickness). The the density constant  $\rho_0$  is determined by the condition

$$\int \rho(r) d^3r = A_c, \quad (32)$$

where  $A_c$  is the mass of the core in units of nucleon mass. The value of  $a$  and  $r_0$  are chosen following suggestions in the literature [10]. The phenomenological  $\Lambda N$  potential is given by

$$V_{\Lambda N}(r) = V_0 \exp(-r^2/\eta^2) \quad (33)$$

with  $V_0$  and  $\eta$  adjusted to reproduce the experimental binding energy ( $B_\Lambda$ ) of single- $\Lambda$  hypernuclei (see Table II) in the core- $\Lambda$  subsystem. Then the core- $\Lambda$  potential is given by

$$V_{c\Lambda}(r) = \int \rho(r_1) V_{\Lambda N}(|\vec{r}_1 - \vec{r}|) d^3r_1. \quad (34)$$

A two dimensional plot of the  $\Lambda\Lambda$ , effective  $\Lambda N$  and core- $\Lambda$  folded potential are shown in Fig. 2. The lowest eigen values ( $\omega_0$ ) of the three body effective potential is plotted against the hyper-radial distance  $\rho$  as shown in Fig. 3.

The strength of  $\Lambda N$  potential is expected to be weakened with the increase in mass of the core due to the screening or shielding effect by neighboring nucleons within the core when the interacting nucleon is embedded in the core. The  $\pi$ -mesic decay of  $\Lambda$  hyperon ( $\Lambda \rightarrow N + \pi$ ) is predominant in the free space but tends to be suppressed in hypernucleus by the Pauli-exclusion principle and instead nonmesic weak process ( $\Lambda + N \rightarrow N + N$ ) becomes dominant with increasing mass number [7,47-51]. Thus we actually get an effective  $\Lambda N$  interaction by the folding process. The parameters of this effective  $\Lambda N$  potential are listed in Table II. The variation of the depth of the effective  $\Lambda N$  interaction against the core mass ( $A_c$ ) is displayed in Fig. 4.

The truncated set of CDE for a given  $K_{max}$  takes the form

$$\begin{aligned} & \left[ -\frac{\hbar^2}{2\mu} \left( \frac{d^2}{d\rho^2} - \frac{\mathcal{L}_K(\mathcal{L}_K+1)}{\rho^2} \right) - E \right] U_{Kl_{x_1}LS}(\rho) \\ & + \sum_{K'=0,2,\dots}^{K_{max}} \sum_{l'_{x_1} (allowed)} U_{K'l'_{x_1}LS}(\rho) = 0 \end{aligned} \quad (35)$$

(allowed  $l'_{x_1}=0, 2, \dots$  only for  $S=0, L=0$ ). Note that the subscripts  $l_{y_1}$  ( $=l_{x_1}$ ) or  $l'_{y_1}$  ( $=l'_{x_1}$ ) have been suppressed for brevity. Eq. (12) is solved to get the ground state energy

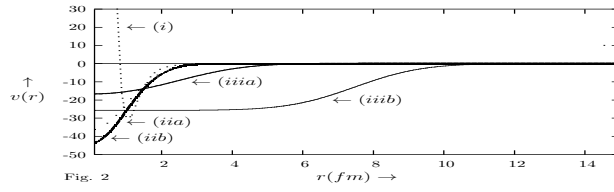


Figure 2: Plot of: (i)  $\Lambda\Lambda$  potential; (ii) effective  $\Lambda N$  potential for  ${}^6_{\Lambda\Lambda}\text{He}$ ; (iii) effective  $\Lambda N$  potential for  ${}^{92}_{\Lambda\Lambda}\text{Zr}$ ; (iv) core- $\Lambda$  folded potential for  ${}^6_{\Lambda\Lambda}\text{He}$ ; (v) core- $\Lambda$  folded potential for  ${}^{92}_{\Lambda\Lambda}\text{Zr}$ ; ( $v$  is in MeV and  $r$  is the relative separation)

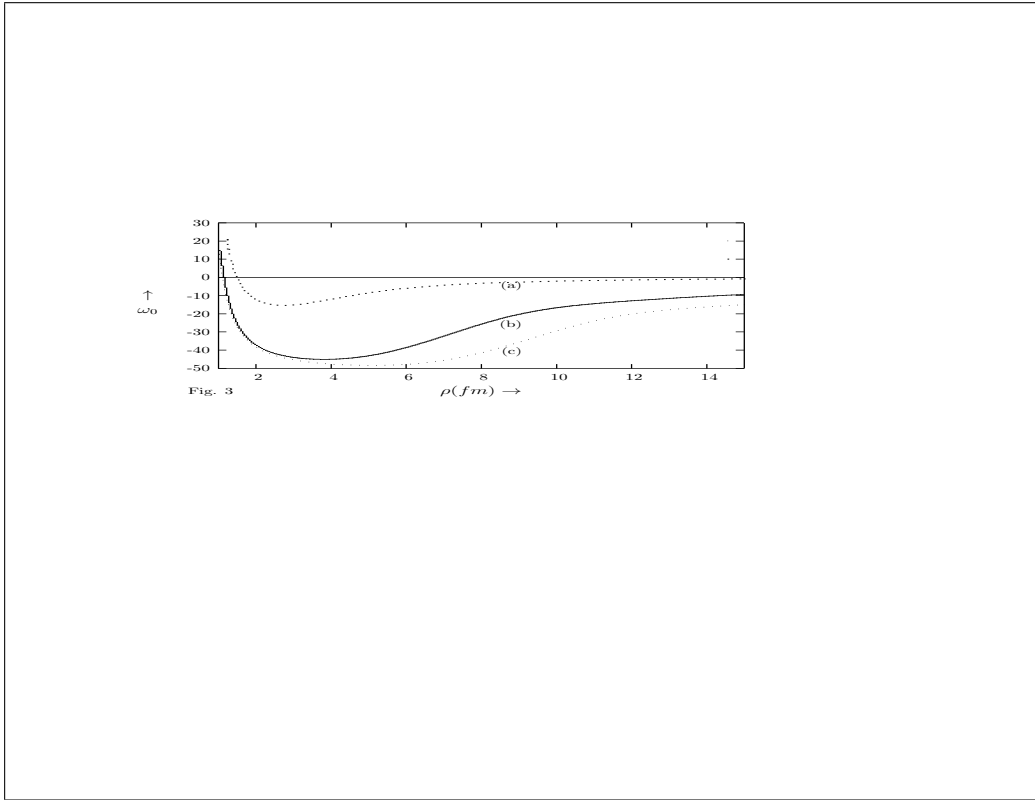


Figure 3: Plot of lowest eigen potential  $\omega_0(\text{MeV})$  against hyperradial distance  $\rho$  for double- $\Lambda$  hypernuclei (a)  ${}^6_{\Lambda\Lambda}\text{He}$ , (b)  ${}^{42}_{\Lambda\Lambda}\text{Ca}$  and (c)  ${}^{92}_{\Lambda\Lambda}\text{Zr}$

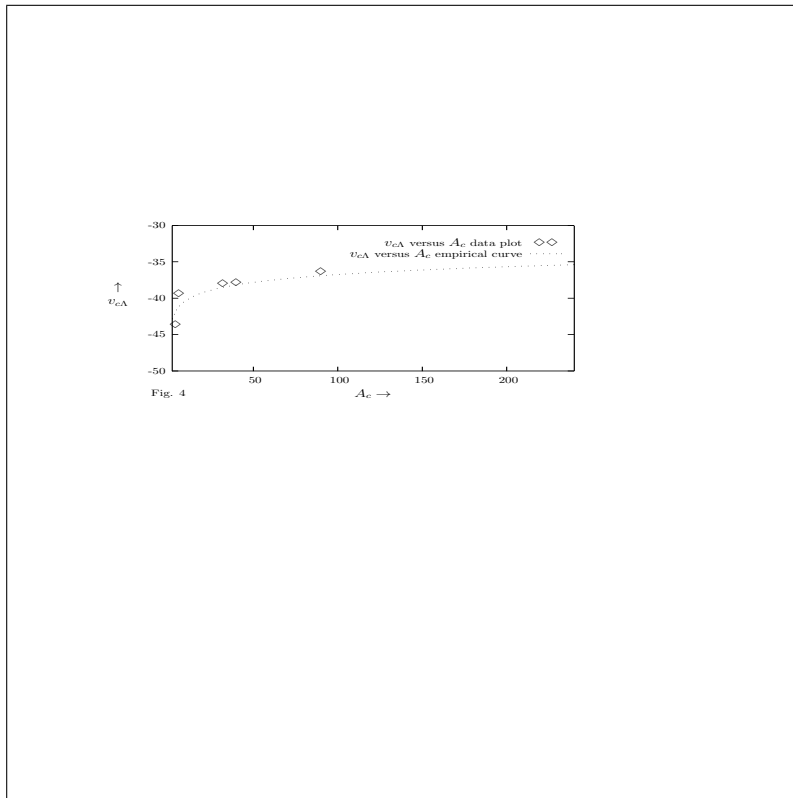


Figure 4: Plot of core- $\Lambda$  potential depth  $v_{c\Lambda}(\text{MeV})$  against mass of core ( $A_c$ )

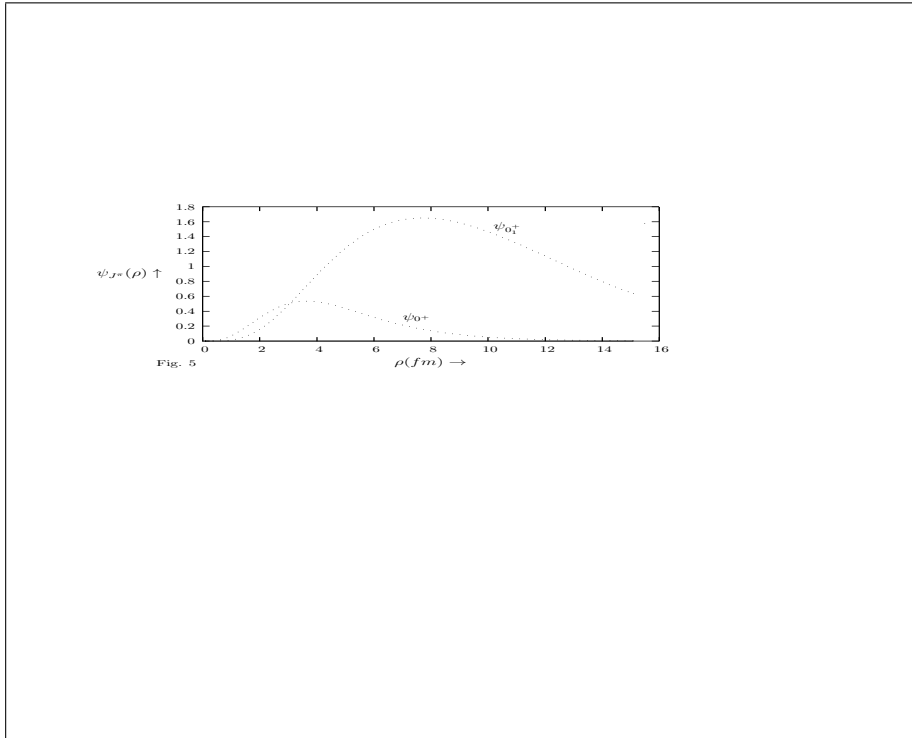


Figure 5: Plot of ground and excited state wavefunctions for  ${}^6_{\Lambda\Lambda}\text{He}$

$E_{(0)}$  and wave functions  $U_{K\alpha_1}^{(0)}$ , by the hyperspherical adiabatic expansion (HAA). For the single- $\Lambda$  hypernuclei, we solve Eq. (14) with  $V(\rho)$  replaced by  $V_{c\Lambda}(\rho)$  plus centrifugal potential. The results are presented in the last two columns of Table II. For double- $\Lambda$  hypernuclei, we use the same  $V_{c\Lambda}$  and solve Eq. (12) for the ground state. Then following the prescription of sec. II, we obtain the energy and wavefunction of the higher excited states. The ground and excited state wave functions for  ${}^6_{\Lambda\Lambda}\text{He}$ ,  ${}^{42}_{\Lambda\Lambda}\text{Ca}$ , and  ${}^{92}_{\Lambda\Lambda}\text{Zr}$  are respectively shown in Fig. 5, 6 and 7. The calculated values of two- $\Lambda$  separation energy ( $B_{\Lambda\Lambda}$ ) at  $K_{max} = 20$  for the ground state (ie.  $0^+$ ), different excited states (ie.  $0_1^+$ ,  $0_2^+$ ,  $0_3^+$ , etc) and  $\Lambda\Lambda$  bond energy ( $\Delta B_{\Lambda\Lambda}$ ) for the ground state of  ${}^6_{\Lambda\Lambda}\text{He}$ ,  ${}^8_{\Lambda\Lambda}\text{Be}$ ,  ${}^8_{\Lambda\Lambda}\text{He}$ ,  ${}^{34}_{\Lambda\Lambda}\text{S}$ ,  ${}^{42}_{\Lambda\Lambda}\text{Ca}$ ,  ${}^{92}_{\Lambda\Lambda}\text{Zr}$  are presented in Table III. The variation of the single- $\Lambda$  separation energy  $B_{\Lambda}$  with the mass of the core  $A_c$  is shown in Fig. 8. On the same graph, the variation of the two- $\Lambda$  separation energy  $B_{\Lambda}$  with the mass  $A$  is also plotted. The calculated two- $\Lambda$  separation energy ( $B_{\Lambda\Lambda}$ ) and  $\Lambda\Lambda$  bond energy ( $\Delta B_{\Lambda\Lambda}$ ) of  ${}^6_{\Lambda\Lambda}\text{He}$  are in agreement with the experimental value  $7.25 \pm 0.19 \text{ MeV}$  [7] and  $1.01 \text{ MeV}$  [7] respectively. The predicted two- $\Lambda$  separation energies for the ground and excited states of all the six double- $\Lambda$  hypernuclei considered here are depicted in the energy level diagram (see Fig. 9).

After obtaining the three body wave function by the HHE approach, root mean square (rms) matter radius ( $R_M$ ) of the three-body system has been calculated following the equation

$$R_M = \left[ \frac{A_c R_c^2 + m_{\Lambda} \langle r_{13}^2 + r_{12}^2 \rangle}{A_c + 2m_{\Lambda}} \right]^{1/2}, \quad (36)$$

where  $A_c$ ,  $m_{\Lambda}$  are the masses of the core and the  $\Lambda$  hyperon (in units of nucleon mass) and  $R_c$  is the matter radius of the core determined by the relation  $R_c = r_0 A_c^{1/3}$  with  $r_0 = 1.70 \text{ fm}$ . The rms core- $\Lambda$  separation is defined as

$$R_{c\Lambda} = \left[ \frac{\langle r_{13}^2 + r_{12}^2 \rangle}{2} \right]^{1/2}. \quad (37)$$

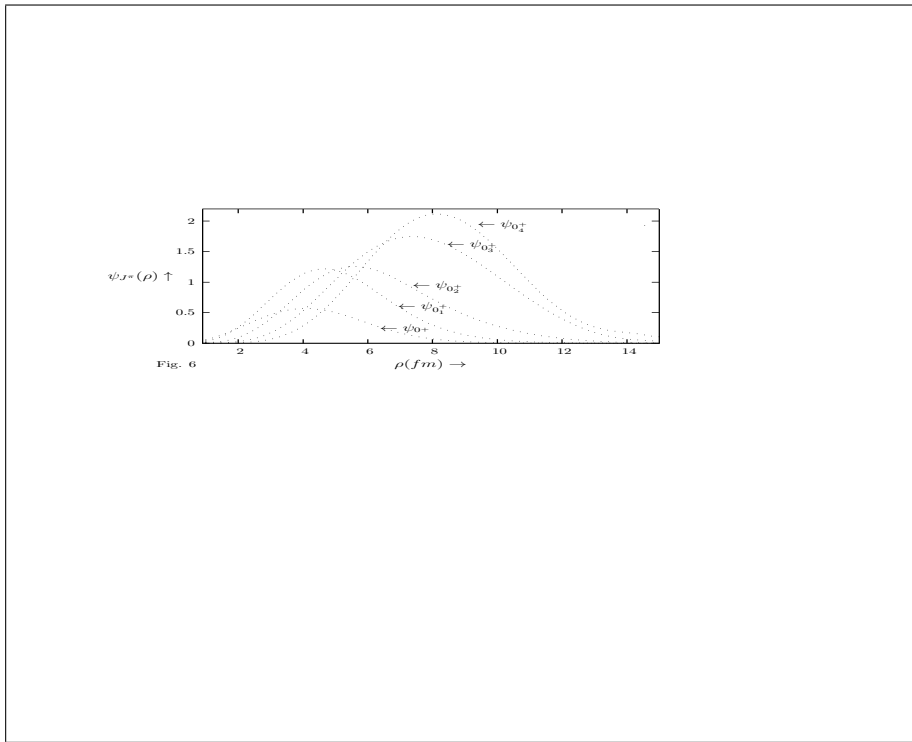


Figure 6: Plot of ground and excited state wavefunctions for  ${}_{\Lambda\Lambda}^{42}\text{Ca}$

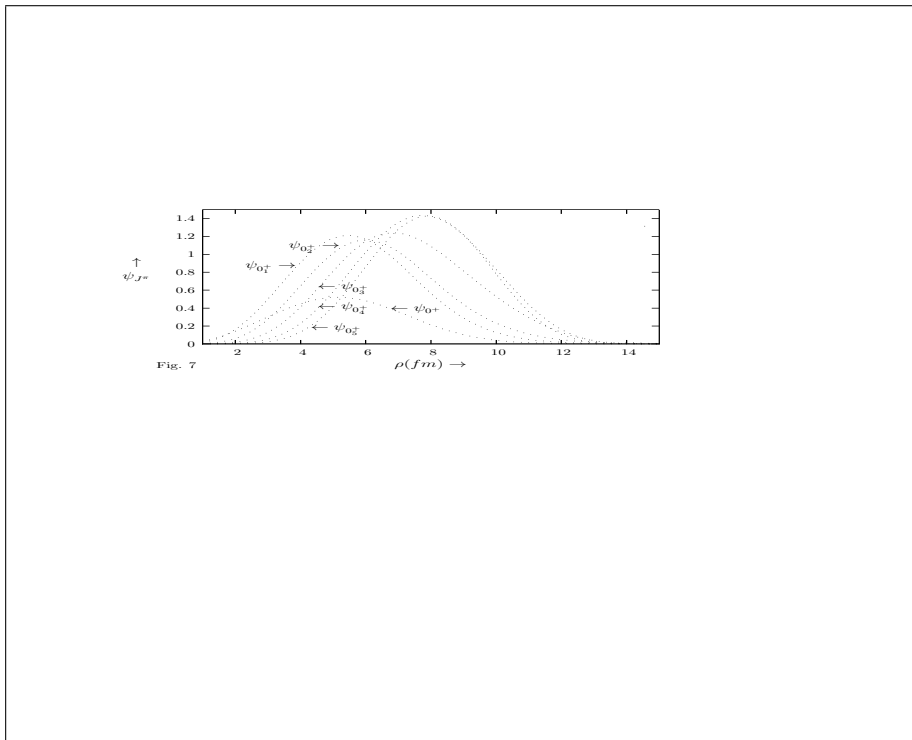


Figure 7: Plot of ground and excited state wavefunctions for  ${}_{\Lambda\Lambda}^{92}\text{Zr}$

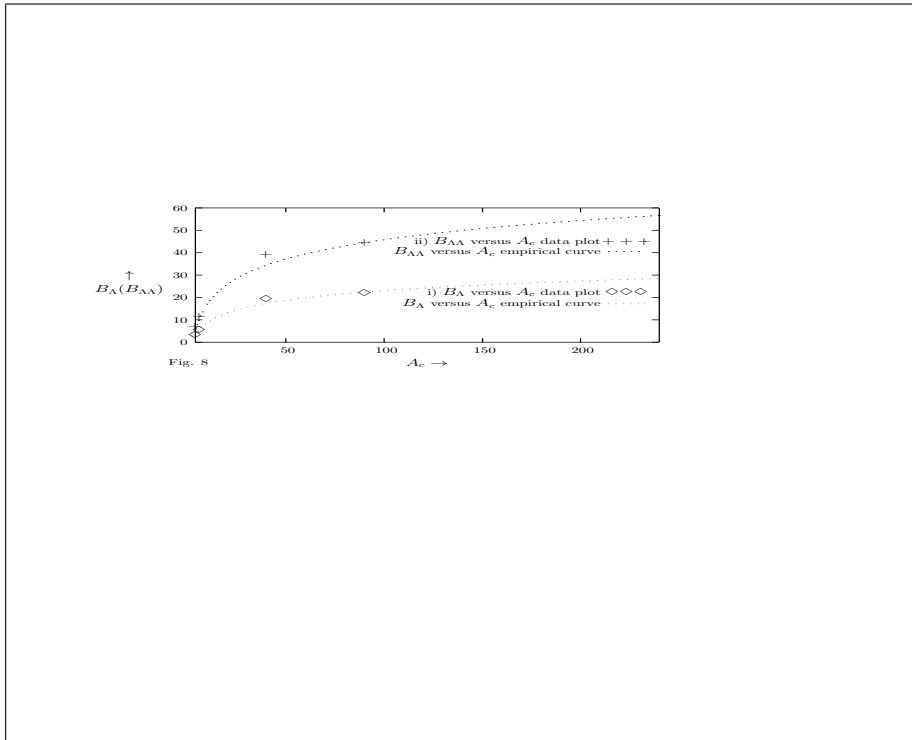


Figure 8: Plot of ground state- (i) Single- $\Lambda$  separation energy  $B_\Lambda$ (MeV) and (ii) Two- $\Lambda$  separation energy  $B_{\Lambda\Lambda}$  (MeV), against mass of the core  $A_c$

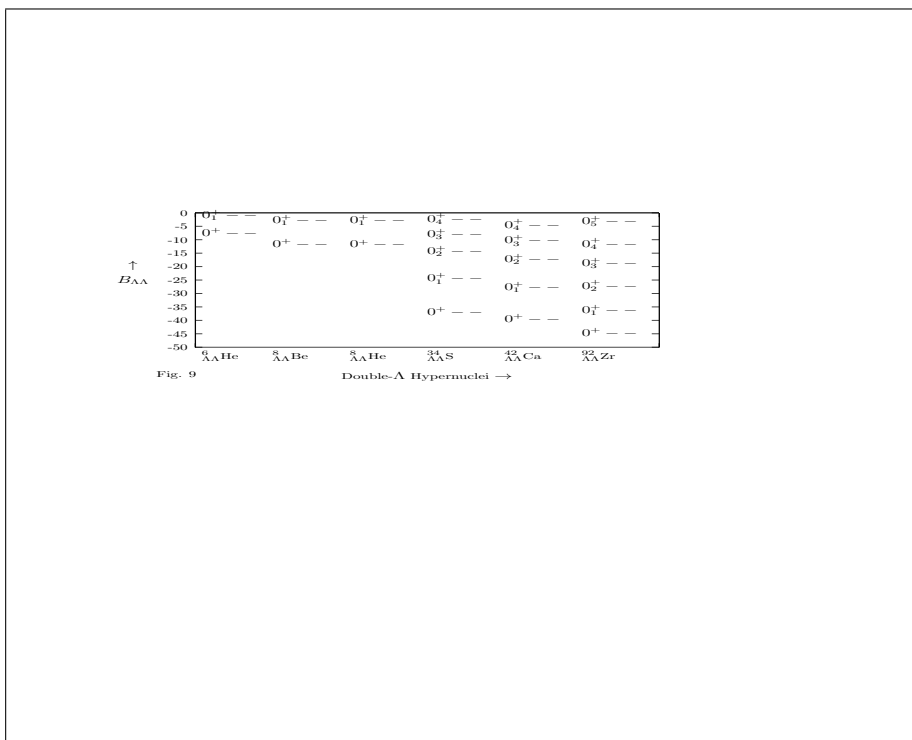


Figure 9: Energy Level diagram of Double- $\Lambda$  Hypernuclei [ $B_{\Lambda\Lambda}$  is in MeV]

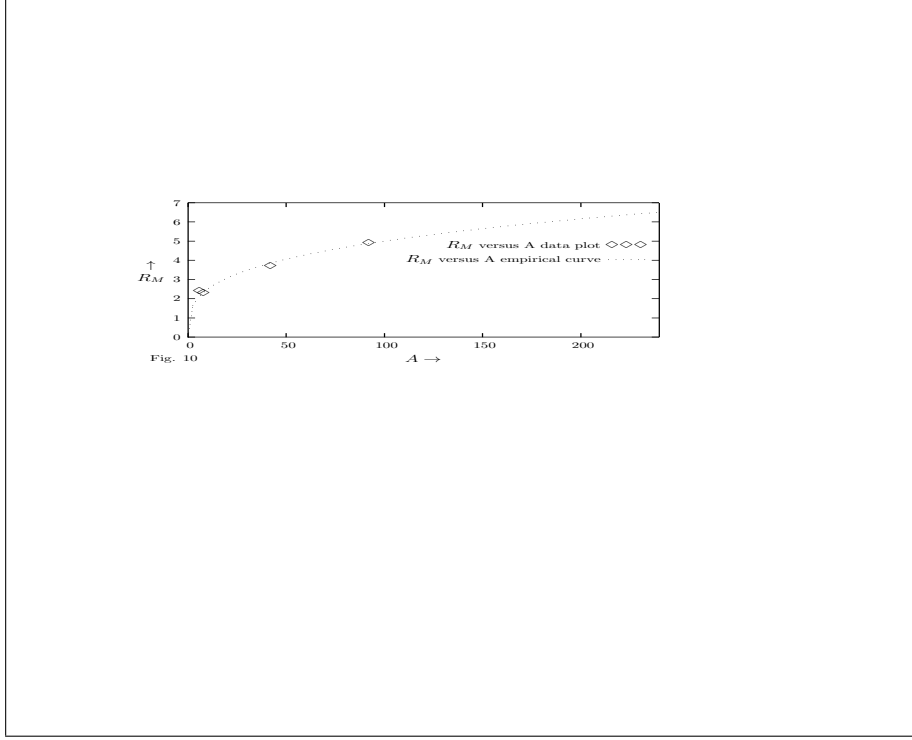


Figure 10: Variation of ground state rms matter radius  $R_M$  (fm) with mass  $A$  (in nucleon mass unit) of the double- $\Lambda$  hypernuclei

The expectation value of the observable  $\langle r_{13}^2 + r_{12}^2 \rangle$  is given by the expression

$$\begin{aligned} \langle r_{13}^2 + r_{12}^2 \rangle &= \sum_{KK'l_{x_1}LS} \int_0^\infty \rho^2 d\rho U_{Kl_{x_1}LS}(\rho) U_{K'l_{x_1}LS}(\rho) \int_0^{\pi/2} ({}^{(2)}P_K)^{l_{x_1}, l_{x_1}}(\Phi) ({}^{(2)}P_{K'})^{l_{x_1}, l_{x_1}}(\Phi) \\ &\times \left[ \frac{1}{2a_{23}^2} \cos^2\Phi + \frac{2}{a_{(23)1}^2} \sin^2\Phi \right] \cos^2\Phi \sin^2\Phi d\Phi. \end{aligned} \quad (38)$$

The rms separation between the valence  $\Lambda$ -hyperons ( $R_{\Lambda\Lambda}$ ) is given by the expression

$$R_{\Lambda\Lambda} = \left[ \langle r_{23}^2 \rangle \right]^{1/2}, \quad (39)$$

where

$$\begin{aligned} \langle r_{23}^2 \rangle &= \frac{1}{a_{23}^2} \sum_{KK'l_{x_1}LS} \int_0^\infty \rho^2 d\rho U_{Kl_{x_1}LS}(\rho) U_{K'l_{x_1}LS}(\rho) \\ &\times \int_0^{\pi/2} ({}^{(2)}P_K)^{l_{x_1}, l_{x_1}}(\Phi) ({}^{(2)}P_{K'})^{l_{x_1}, l_{x_1}}(\Phi) \cos^4\Phi \sin^2\Phi d\Phi. \end{aligned} \quad (40)$$

The result of these calculations are recorded in Table IV. The variation of the ground state rms matter radius ( $R_M$ ) with mass number ( $A$ ) of the double- $\Lambda$  hyper nuclei is displayed in Fig. 10.

Finally we have calculated the contribution of various orbital angular momenta  $l_{x_1}$  at  $K_{max} = 20$  to the ground state probability density distribution to identify the dominating component of the partial waves, and the results are presented in Table V.

## IV Summary and Conclusion

Since hyperons and nucleons both have three quark (qqq) structure (eg.  $p \rightarrow uud$ ,  $n \rightarrow udd$ ,  $\Lambda^0 \rightarrow uds$  etc.) interactions among hyperons as well as with nucleons should

give valuable inputs to the knowledge of strong interactions. But not much attention has so far been directed to the study of hyperon-hyperon and hyperon-nucleon interaction through the critical investigation of hypernuclei. We have undertaken a systematic study of the bound state properties of few light and medium mass hypernuclei to gather some idea about nature of hyperon-hyperon and hyperon-nucleon interactions and the internal structure of the three-body systems. The hyperspherical harmonics expansion (HHE) method adopted here is an essentially exact method, where calculations can be carried out up to any desired precision by gradually increasing the expansion basis. For  ${}^6_{\Lambda\Lambda}\text{He}$ , the calculated two- $\Lambda$  separation energy  $B_{\Lambda\Lambda}$  and  $\Lambda\Lambda$  bond energy  $\Delta B_{\Lambda\Lambda}$  (see Table III) both at  $K_{max} = 20$  are well within the experimental error limits  $7.25 \pm 0.19\text{MeV}$  [7] and  $1.01\text{MeV}$  [7]. Both values are less than our previous calculation [52] done by using old data of [5]. The strength of the core- $\Lambda$  potential for a fixed range parameter ( $\eta$ ), is found to become weaker as the mass of the core increases. And this trend is found to fit a logarithmic function of the form

$$v_0(A_c) = \delta_1 \log_e(A_c) + \delta_2 \quad (41)$$

with  $\delta_1 = 1.55033\text{MeV}$  and  $\delta_2 = -43.8843\text{MeV}$ . In the low mass region  $v_0$  decreases faster than in the mid mass range before achieving saturation in the heavier mass region. This phenomenon may be viewed as the effect of screening of the interacting nucleon embedded in the core, by the surrounding nucleons. And this effect of screening increases as the number of neighboring nucleons increases. One may expect such a result from physical intuition. Following the above empirical formula one can estimate the depth of the effective  $\Lambda N$  potential for the single- $\Lambda$  hypernuclei in any mass range. The single  $\Lambda$  separation energy  $B_\Lambda$  is found to increase with the increase in core mass approximately following the equation

$$B_\Lambda(A_c) = \delta_3 \log_e(A_c) + \delta_4 \quad (42)$$

with  $\delta_3 = 6.21483\text{MeV}$  and  $\delta_4 = -5.55812\text{MeV}$ . Similarly, the trend of variation of the two- $\Lambda$  separation is found to follow the equation

$$B_{\Lambda\Lambda}(A) = \delta_5 \log_e(A) + \delta_6 \quad (43)$$

with  $\delta_5 = 12.3892\text{MeV}$  and  $\delta_6 = -11.2555\text{MeV}$ . Thus Eq. (42) and (43) may respectively be useful in determining  $B_\Lambda$  and  $B_{\Lambda\Lambda}$  for any one- and two  $\Lambda$  hypernuclei. Also the approximate size of any double  $\Lambda$  hypernuclei of mass number ( $A$ ) can be estimated by our empirical formula

$$R_M(A) = \delta_7 A^{\delta_8} \quad (44)$$

with  $\delta_7 = 1.25244\text{fm}$  and  $\delta_8 = 0.300609\text{fm}$ . It can be seen from energy level diagram (see Fig. 9) that the energy levels for the exotic isobars  $\Lambda\Lambda^8\text{He}$  and  $\Lambda\Lambda^8\text{Be}$  are almost identical. However the slight difference in their one- and two- $\Lambda$  separation energies (see Column 4 of Table II and III) is due to the relatively stronger Coulomb repulsion in the core of the latter. The calculated values of the partial probability (see Table V) shows that larger contribution to the ground state total wave function comes from the  $l_{x_1} = 0$  partial wave and the rest comes from the higher even  $l_{x_1}$  components. The contribution from the odd  $l_{x_1}$  values are zero. From the calculated values of the single- and double-  $\Lambda$  separation energies (see Table II & III) and the rms matter radii (see Table IV) it may be concluded that the addition of one- or two- $\Lambda$  particle to the core makes the system strongly bound and more compact. This is quite true as the weakly bound  ${}^6\text{He}$  or unbound  ${}^6\text{Be}$  core becomes strongly bound on addition of one or two  $\Lambda$  hyperon(s). Hence, it is quite possible that our predictions for the binding energies of the ground and excited states of experimentally unobserved double  $\Lambda$  hypernuclei are valid. Thus we may say that the  $\Lambda N$  force is much stronger and much attractive than the  $NN$  force. Perhaps this may be due to the presence of the strange quark in the  $\Lambda$  hyperon quark constituents.

**Acknowledgments** The author gratefully acknowledges computer facilities provided by the Department of Physics, Aliah University.

## References

- [1] M. Danysz et al., Nucl. Phys. **49**, 121(1963).
- [2] D. J. Prowse, Phys. Rev. Lett. **17**, 782(1966).
- [3] R. H. Dalitz, D. H. Davis, P. H. Fowler, A. Montwill, J. Poriewski, and J. A. Zakrzewski, Proc. R. Soc. London, Ser. **A426**, 1(1989).
- [4] D. H. Davis, Nucl. Phys. **A754** 3c(2005); R. H. Dalitz, Nucl. Phys. **A754** 4c(2005).
- [5] H. Himeno et al., Prog. Theo. Phys. **Vol. 89**, No. 1, 109(1993).
- [6] L. Majling, Nucl. Phys. **A585**, 211c(1995).
- [7] Takahashi et. al., Phys. Rev. Lett. **87**, 212502(2001).
- [8] S. Aoki et al., Prog. Theo. Phys. **85**, 1287(1991).
- [9] H. Nemura, Y. Suzuki, Y. Fuziwara and C. Nakamoto, Prog. Theo. Phys. **Vol. 105**, No. 5, 929(2000).
- [10] R. R. Roy and B. P. Nigam, Nuclear Physics Theory and Experiment, Fifth Wiley Eastern Reprint, February (1993)pp-389; J. Caro et al., Nucl. Phys. **A646**, 299(1999).
- [11] Y. Yamamoto et al., Nucl. Phys. **A547**, 233c(1992).
- [12] A. Gal, Advances in Nucl. Phys., eds. M. Baranger and E. Vogt. **Vol.8**, 1(1975, Plenum).
- [13] G. Alexander et al., Phys. Rev. **173**, 1452(1968).
- [14] B. Sechi - Zorn et al., Phys. Rev. **175**, 1735(1968).
- [15] J. A. Kadyk et al., Nucl. Phys. **B27**, 13(1971).
- [16] J. M. Hauptman, LBL Report No. **LBL-3608**(1974).
- [17] F. Eisele et al., Phys. Lett. **37B**, 204(1971).
- [18] R. Engelmann et al., Phys. Lett. **21**, 487(1966).
- [19] Y. C. Tang and R. C. Herndon, Nuovo Cimento **XLVIB**, N.1., 117(1966).
- [20] R. H. Dalitz and G. Rajasekaran, Nucl. Phys. **50**, 450(1964).
- [21] S. Ali and A. R. Bodmer, Phys. Lett. **24B**, 343(1967).
- [22] A. R. Bodmer, Q. N. Usmani, and J. Carlson, Nucl. Phys. **A422**, 510(1984).
- [23] H. Bando, T. Motoba and Z. J. Zofka, Int. J. Mod. Phys. **A5**, 4021(1990); see references therein.
- [24] G. A. Lalazissis, M. E. Grypeos, and S. E. Massew, Phys. Rev. **C37**, 2098(1988).

- [25] Y. Yamamoto, T. Motoba, H. Himeno, K. Ikeda, and S. Nagata, Prog. Theor. Phys. Suppl. **117**, 361(1994).
- [26] C. D. Lin, Phys. Rep. **257**, 1(1995).
- [27] T. H. Gronwall, Phys. Rev. **51**, 655(1937).
- [28] J. Macek, J. Phys. **B 1**, 831(1968).
- [29] J. L. Ballot and J. Navarro, J. Phys.**B 8**, 172(1975).
- [30] V. D. Efros, A. M. Frolov and M. I. Mukhtarova, J. Phys.**B 15**, 1819(1982).
- [31] T. K. Das, R. Chattopadhyay and P. K. Mukherjee, Phys. Rev. A50, 3521(1994).
- [32] R. Chattopadhyay and T. K. Das, Phys. Rev. **A56**, 1281(1997).
- [33] Md. A. Khan, S. K. Datta, and T. K. Das, FIZIKA B (Zagreb)**8**, 4, 469(1999).
- [34] T. K. Das, H. T. Coelho and M. Fabre de la Ripelle, Phys. Rev. **C26**, 2288(1982).
- [35] Khan M. A., Dutta S. K., Das T. K. and Pal M. K., J. Phys. G: Nucl. Part. Phys. **24**, 1519(1998).
- [36] Yu. A. Simonov, Yad. Fiz. **3**, 630(1960) [Sov. J. Nucl. Phys. **3**, 461(1960)]; in proced. of the international symposium on the present status and novel developments in the nuclear many body problem. Rome, 1972, edited by F. Calogera and C. Ciofi Degli Atti (Editrice composition, Bologna, 1973), p527; Sov. J. Nucl. Phys. **7**, 722(1968).
- [37] F. Zernike, H. C. Brinkman, Proc. Kon. Acad. Wtensch, **33**, 3(1975).
- [38] M. Fabre de la Ripelle, Proc. Int. Sch. Nucl. Theo. Phys., Predeal 1969.
- [39] M. Fabre de la Ripelle, Comp. Reend. Acad. Sci., **269B**, 80(1970); **273A**, 1007(1971).
- [40] J. L. Ballot and M. Fabre de la Ripelle, Ann. Phys. ( N. Y.) **127**, 62(1980).
- [41] J. M. Richard, Phys. Rep. **212**, 1(1992).
- [42] H. Leeb, H. Fiedeldey, E. G. O. Gavin, S. A. Sofianos and R. Lipperheide, Few Body Systems **12**, 55(1992).
- [43] N. Barnea and A. Novoselsky, Ann. Phys. ( N. Y.) **256**, 192(1997).
- [44] S. Watanabe, Y. Hosoda and D. Kato, J. Phys. **B26**, L495(1993).
- [45] F. Cooper, A. Khare and U. Sukhatme, Phys. Rep. **251**, 267(1995).
- [46] T. K. Das, H. T. Coelho and M. Fabre de la Ripelle, Phys. Rev. **C26**, 2281(1982).
- [47] R. H. Dalitz and L. Liu, Phys. Rev **116**, 1312(1959).
- [48] M. M. Block and R. H. Dalitz, Phys. Rev. Lett. **11**, 96(1963).

**Table I. Parameters of  $\Lambda\Lambda$  interaction.**

$i \rightarrow$	1	2	3
$\beta_i(fm)$	1.5	0.90	0.5
$V_i(MeV)$	-8.967	-142.385	880.700

- [49] J. B. Adams, Phys. Rev. **156**, 1611(1967).
- [50] C. Y. Chung, D. P. Heddle and L. S. Kisslinger, Phys. Rev. **C27**, 335(1983).
- [51] B. H. Mc Kellar and B. F. Gibson Proc. Int. Conf. on Hypernuclear and Kaon Physics, 1982, Heidelberg, ed. B. Povh, p-156; Phys. Rev. **C30**, 322(1984).
- [52] M. A. Khan and T. K. Das, Pramana- J. Phys, **56** No.1, 57(2001).

## V Figure Caption

1. **Fig. 1** Choice of Jacobi coordinates for the partition 1.
2. **Fig. 2** Plot of: (i)  $\Lambda\Lambda$  potential; (iia) effective  $\Lambda N$  potential for  ${}^6_{\Lambda\Lambda}\text{He}$ ; (iib) effective  $\Lambda N$  potential for  ${}^{92}_{\Lambda\Lambda}\text{Zr}$ ; (iia) core- $\Lambda$  folded potential for  ${}^6_{\Lambda\Lambda}\text{He}$ ; (iib) core- $\Lambda$  folded potential for  ${}^{92}_{\Lambda\Lambda}\text{Zr}$ ; ( $v$  is in MeV and  $r$  is the relative separation)
3. **Fig. 3** Plot of lowest eigen potential  $\omega_0(MeV)$  against hyperradial distance  $\rho$  for double- $\Lambda$  hypernuclei (a)  ${}^6_{\Lambda\Lambda}\text{He}$ , (b)  ${}^{42}_{\Lambda\Lambda}\text{Ca}$  and (c)  ${}^{92}_{\Lambda\Lambda}\text{Zr}$
4. **Fig. 4** Plot of core- $\Lambda$  potential depth  $v_{c\Lambda}(MeV)$  against mass of core ( $A_c$ )
5. **Fig. 5** Plot of ground and excited state wavefunctions for  ${}^6_{\Lambda\Lambda}\text{He}$
6. **Fig. 6** Plot of ground and excited state wavefunctions for  ${}^{42}_{\Lambda\Lambda}\text{Ca}$
7. **Fig. 7** Plot of ground and excited state wavefunctions for  ${}^{92}_{\Lambda\Lambda}\text{Zr}$
8. **Fig. 8** Plot of ground state- (i) Single- $\Lambda$  separation energy  $B_\Lambda(MeV)$  and (ii) Two- $\Lambda$  separation energy  $B_{\Lambda\Lambda}$  (MeV), against mass of the core  $A_c$
9. **Fig. 9** Energy Level diagram of Double- $\Lambda$  Hypernuclei [ $B_{\Lambda\Lambda}$  is in MeV]
10. **Fig. 10** Variation of ground state rms matter radius  $R_M$  (fm) with mass  $A$  (in nucleon mass unit) of the double- $\Lambda$  hypernuclei

## VI Tables

Table II. Parameters of the  $\Lambda N$  potential and corresponding  $\Lambda$  separation energy in the core- $\Lambda$  subsystems.

System	$\Lambda$ -N potential parameters		$B_\Lambda(MeV)$	
			Ground state	
	$V_0(MeV)$	$\chi(fm)$	Expt.	Calc.
${}^5_\Lambda\text{He}$	-43.6102	1.41	$3.12 \pm 0.02$ [12, 23]	3.1200
${}^7_\Lambda\text{He}$	-39.6328	1.41	$5.23 \pm 0.00$ [22]	5.2300
${}^7_\Lambda\text{Be}$	-39.3650	1.41	$5.16 \pm 0.08$ [23]	5.1600
${}^{33}_\Lambda\text{S}$	-38.0436	1.41	$17.96 \pm 0.00$ [24]	17.9600
${}^{41}_\Lambda\text{Ca}$	-37.8497	1.41	$19.24 \pm 0.00$ [24]	19.2400
${}^{91}_\Lambda\text{Zr}$	-36.3328	1.41	$22.10 \pm 0.30$ [25]	22.1000

Table III. Two- $\Lambda$  separation energy in the ground and excited states of different double- $\Lambda$  hypernuclei at  $K_{max} = 20$ .

Hypernuclei	Bound State $J^\pi$	$B_{\Lambda\Lambda}(MeV)$		$\Delta B_{\Lambda\Lambda}(MeV)$	
		Expt.	Calc.	Expt.	Calc.
${}^6_{\Lambda\Lambda}\text{He}$	$0^+$	$7.25 \pm 0.19$ [4]	7.2501	$1.01$ [4]	1.0101
	$0^+_1$	-	0.8613	-	-
${}^8_{\Lambda\Lambda}\text{He}$	$0^+$	-	11.5815	-	1.1215
	$0^+_1$	-	2.7056	-	-
${}^8_{\Lambda\Lambda}\text{Be}$	$0^+$	-	11.4344	-	1.1144
	$0^+_1$	-	2.6451	-	-
${}^{34}_{\Lambda\Lambda}\text{S}$	$0^+$	-	36.7957	-	0.8757
	$0^+_1$	-	24.4038	-	-
	$0^+_2$	-	14.1298	-	-
	$0^+_3$	-	07.9952	-	-
	$0^+_4$	-	02.1448	-	-
${}^{42}_{\Lambda\Lambda}\text{Ca}$	$0^+$	-	39.2357	-	0.7557
	$0^+_1$	-	27.5745	-	-
	$0^+_2$	-	17.0814	-	-
	$0^+_3$	-	10.2213	-	-
	$0^+_4$	-	04.3325	-	-
${}^{92}_{\Lambda\Lambda}\text{Zr}$	$0^+$	-	44.5463	-	0.3463
	$0^+_1$	-	36.1553	-	-
	$0^+_2$	-	27.0817	-	-
	$0^+_3$	-	18.6847	-	-
	$0^+_4$	-	11.4110	-	-
	$0^+_5$	-	03.0006	-	-

Table IV. The r.m.s. matter radii of the ground and excited states of different double- $\Lambda$  hypernuclei at  $K_{max} = 20$ .

Hypernuclei	Bound State $J^\pi$	$R_A(fm)$	$R_{c\Lambda}(fm)$	$R_{\Lambda\Lambda}(fm)$	$R_{(\Lambda\Lambda)c}(fm)$
${}^6_{\Lambda\Lambda}\text{He}$	$0^+$	2.3842	3.1804	4.1437	2.4130
	$0_1^+$	2.7823	3.9536	5.2301	2.9652
${}^8_{\Lambda\Lambda}\text{He}$	$0^+$	2.2939	2.9081	3.8697	2.1711
	$0_1^+$	2.4952	3.4427	4.6361	2.5453
${}^8_{\Lambda\Lambda}\text{Be}$	$0^+$	2.2970	2.9167	3.8810	2.1775
	$0_1^+$	2.5005	3.4560	4.6542	2.5552
${}^{34}_{\Lambda\Lambda}\text{S}$	$0^+$	3.4592	2.9783	4.0864	2.1670
	$0_1^+$	3.4666	3.0998	4.2331	2.2647
	$0_2^+$	3.4840	3.3706	4.6237	2.4528
	$0_3^+$	3.5095	3.7331	5.1750	2.6909
	$0_4^+$	3.5377	4.0998	5.7564	2.9196
${}^{42}_{\Lambda\Lambda}\text{Ca}$	$0^+$	3.7286	3.1140	4.2798	2.2623
	$0_1^+$	3.7332	3.2124	4.3931	2.3441
	$0_2^+$	3.7450	3.4484	4.7293	2.5099
	$0_3^+$	3.7628	3.7779	5.2220	2.7305
	$0_4^+$	3.7830	4.1209	5.7556	2.9496
${}^{92}_{\Lambda\Lambda}\text{Zr}$	$0^+$	4.9045	3.8392	5.3125	2.7720
	$0_1^+$	4.9049	3.8581	5.3148	2.7969
	$0_2^+$	4.9078	4.0007	5.5133	2.8994
	$0_3^+$	4.9124	4.2110	5.8141	3.0466
	$0_4^+$	4.9179	4.4546	6.1672	3.2147
	$0_5^+$	4.9230	4.6693	6.4821	3.3612

Table V. The contribution of the orbital angular momenta  $l_{x_1}$  to the probability density in the ground state of double  $\Lambda$ -hypernuclei at  $K_{max} = 20$ .

Hypernuclei	Partial probability $P_{l_{x_1}}$ for $l_{x_1} =$				
	0	1	2	3	4
${}^6_{\Lambda\Lambda}\text{He}$	0.996130	0.000000	0.003854	0.000000	0.000016
${}^8_{\Lambda\Lambda}\text{He}$	0.997786	0.000000	0.002210	0.000000	0.000003
${}^8_{\Lambda\Lambda}\text{Be}$	0.997757	0.000000	0.002240	0.000000	0.000004
${}^{34}_{\Lambda\Lambda}\text{S}$	0.999900	0.000000	0.000099	0.000000	0.000001
${}^{42}_{\Lambda\Lambda}\text{Ca}$	0.999878	0.000000	0.000121	0.000000	0.000001
${}^{92}_{\Lambda\Lambda}\text{Zr}$	0.999744	0.000000	0.000254	0.000000	0.000002